Phase Unwrapping for Heart and Breathing Rate Estimation Using mmWave FMCW Radar

Seyedeh Fatemeh Mirhosseini[1], Mohammad Alaee-Kerahroodi[1],
Gabriel Beltrao[2], Udo Schroeder[2], Bhavani Shankar M. R.[1]
[1]SnT - Interdisciplinary Centre for Security, Reliability and Trust, University of Luxembourg, Luxembourg
[2]IEE S/A, Luxembourg

***Abstract*—Accurate measurement of heart rate and breathing rate using radar technology requires precise detection of displacements caused by chest wall movements. These vital signs are directly correlated with the displacement information, which is extracted from the phase of the returned radar signal. Consequently, the phase demodulation step is critical for the non-invasive and remote monitoring of these physiological parameters. This paper investigates the accuracy of various phase unwrapping methods through both simulation and real-time measurements using a 60 GHz Frequency Modulated Continuous Wave (FMCW) radar system. Our results demonstrate that with appropriate sampling rate selection, the conventional phase-unwrapping method exhibits superior robustness and reliability compared to alternative approaches for vital sign monitoring applications.**

***Index Terms*—Vital sign monitoring, phase unwrapping, FMCW radar.**

I. Introduction

It has been nearly two decades [1] since wireless sensing circuits and systems for healthcare applications have been active research fields. Remote monitoring of vital signs plays a crucial role in the healthcare observation domain, as in-person schedule monitoring cannot predict or instantly detect a sudden abnormality. Radars can be a good substitute for non-invasively measuring heart rate and breathing rate without connecting sensors, and also with the prevailing privacy of people [2]. Today, in this field, various types of radars such as continuous wave (CW) [3], frequency modulated continuous wave (FMCW) [4], [5] ,and Impulse Radio Ultra-Wideband (IRUWB) [6], [7] are investigated.

The core principle for estimating respiration rate and heart rate using radar lies in the accurate measurement and interpretation of the chest wall movements, which manifest as variations in the phase of the reflected signal [8]–[10]. When the displacement caused by chest movements is a fraction of the radar wavelength, the corresponding phase changes can be observed directly without phase wrapping issues. However, larger displacements introduce phase ambiguity, necessitating effective phase unwrapping techniques to resolve this demodulation challenge. Consequently, various phase unwrapping methods have been proposed to enhance the accuracy and reliability of vital sign monitoring using radar systems.

This research was funded in whole, or in part, by the Luxembourg National Research Fund (FNR), grant reference [IF/18856415/VITALRAD].

Phase Unwrap (PU) mentioned in this research, is unwrapping the result of Arctangent (ATAN) demodulation. However, considering the presence of noise and the calibration requirement, using PU can be inefficient [11]. The differentiate and cross multiply (DACM) method uses summation, subtraction, multiplication, and division. The other methods usually use derivative and integral operands. In DACM, the exact formulation of the arctangent derivative is computed; therefore, it is less prone to discontinuity caused by sudden changes with a large phase amplitude [12]. Modified DACM overcomes the noise effect; however, DC offset cannot be retrieved in this method, and so DC incompatibility leads to phase coupling in the time domain [13]. In [14], the EATAN1 and EATAN2 methods are introduced to enhance the performance of phase demodulation. EATAN1 uses the second-order derivative to identify and correct phase discontinuities and is suitable for both periodic and aperiodic motions. In contrast, EATAN2 is designed specifically for periodic motions, making it more applicable to real-world signal scenarios. Both methods incorporate a phase compensation step as an initial stage to balance the wrapped signal. Although these methods are more efficient than others, inaccuracies in derivative order estimation lead to failures in the recovery procedure. Unlimited Sampling (UnSam) [15] aims to reconstruct the phase under low sampling rate conditions, but shares similar drawbacks with EATAN1 and EATAN2. It requires knowledge of the differentiation level, which is challenging to obtain in radar-based vital sign monitoring applications, and necessitates extensive parameter tuning for real-time use. Current methods that use deep learning algorithms are dependent on the training set, which due to the randomness of the phenomena cannot cover every possible state and is limited to the conditions included in the training set [16], [17]. Moreover, in the case of failure due to a large number of parameters, it is almost impossible to determine the reason [18].

In this paper, we investigate various phase unwrapping methods through both simulation and real-time measurements. We demonstrate that, in many practical scenarios, fine-tuning the parameters for methods based on high-order differentiation is challenging, if not impractical. Consequently, the proposed approach for recovering the phase is selecting an appropriate sampling rate and employing first-order differentiation, and it is a robust and effective phase unwrapping solution.

A. Notations

In this paper, $\lfloor . \rceil$ indicates the "round" that is a converter operator to the nearest integer. $\lfloor . \rfloor$ is an indication to truncate a value to the lowest integer around it, while $\lceil . \rceil$ shows the highest integer after the value. The remainder of the value subtracted from its truncated version is defined as $\mathcal{M}_\lambda : f \rightarrow \left([\![\frac{f}{2\lambda} + \frac{1}{2}]\!] - \frac{1}{2} \right)$ where $[\![f]\!] \stackrel{\text{def}}{=} f - \lfloor f \rfloor$ and $\lambda > 0$ is the folding interval. The above equation is equivalent to $\mathcal{M}_\lambda(f) \equiv f \mod 2\lambda$. We define the index selection operators as $\mathcal{I}_\eta^n(x[n]) = \begin{cases} 0 & x[n] \geq \eta \\ 1 & x[n] < \eta \end{cases}$ and $\mathcal{G}^n(x[n]) = \begin{cases} \lfloor x[n] \rfloor & x[n] \geq 0 \\ \lceil x[n] \rceil & x[n] < 0. \end{cases}$ $\mathcal{S}_k^n = \sum_k^n (.)$ is indicating cumulative summation.

II. System Model and Methods

To estimate vital signs using millimeter wave (mmWave) FMCW radar sensors, various challenges must be addressed, including (a) scalloping loss due to mismatches between human body location and the FFT grid, (b) the phase estimation problem, and (c) Random Body Movement (RBM). Although scallop loss can be mitigated by selecting or combining range bins where a person is located [19], and then extracting the phase of the corresponding range bin, the challenges (b) and (c) are interconnected and form the focus of this paper.

Using FMCW radar, BGT60TR13C [20], we obtain phase information related to respiratory rate and heart rate. In this way, the displacement of the chest wall can be measured. Therefore, the heart rate and the breathing rate are estimated by executing the fast Fourier transform (FFT) of the displacement signal. Selection of the range bin of interest in "fast-time" leads to the signal;

$$y(t) = e^{j\phi(t)}, \tag{1}$$

where t is the slow-time interval equivalent to the chirp repetition time in a FMCW radar. This contains the displacement within its phase. The relation between phase and displacement is [8], [21],

$$\phi(t) = \frac{4\pi x(t)}{\lambda}, \tag{2}$$

where λ is the operating wavelength and $x(t)$ is the displacement signal. $x(t)$ including heartbeat and breathing is affected by RBM which can be retrieved as

$$x(t) = x_h(t) + x_b(t) + x_r(t). \tag{3}$$

Hence, the phase of the exponential is estimated using conventional arctangent demodulation as:

$$\hat{\phi}(t) = \tan^{-1}\{y(t)\}, \tag{4}$$

which has the limitation of codomain $[-\pi, \pi]$. Therefore, if the phase falls out of the mentioned interval, the estimated phase will be wrapped, and the true phase will be lost. Based on $\phi(t) = \frac{4\pi x(t)}{\lambda}$, it is clear that if $x(t)$ changes more than $\lambda/4$, then $\hat{\phi}(t)$ will be wrapped. Since the FMCW radar in this research operates in the 60 GHz frequency range, the value of λ is equal to 5 mm. Meanwhile, the standard range of heartbeat is $60 - 100$ bpm, which is approximately equal to the chest-wall movement of 0.5 mm to 0.2 mm [22], and the breathing movement can increase from 12 mm to 4 mm, which is equal to $5 - 30$ breaths per minute [23]. Using this radar, phase estimation encounters the unwrapping problem, since the value of the phase can exceed the $-\pi$ and $+\pi$ interval as the displacement can surpass $\frac{\lambda}{4} = 1.25$ mm. In addition to the problem indicated in a motionless scenario, the presence of RBM in the range bins of interest leads to an increase of $x(t)$, therefore, more phase ambiguity can occur due to the excess of the codomain and the unwrapping urge.

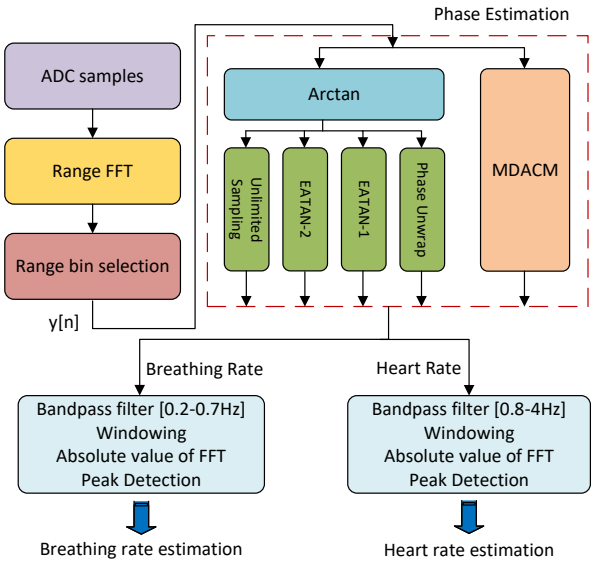

Fig. 1: System model of vital sign monitoring using radar

To address the challenges mentioned above, this paper evaluates the practicality of different phase unwrapping approaches in real-time using an mmWave FMCW radar sensor. The diagram proposed in Fig. 1 illustrates the structure of the algorithms implemented in this investigation, with a primary focus on unwrapping solutions to overcome the mentioned obstacles. Based on the figure, some range bins of interest are selected from the analog to digital converter (ADC) range-FFT samples to reach the slow-time domain, then regarding the decision about phase estimation, one method will be chosen. The recovered phase signal is then filtered and windowed within the frequency ranges of interest: $[0.2, 0.7]$ Hz for the breathing rate and $[0.8, 4]$ Hz for the heart rate. Finally, peak detection is performed on the filtered signal spectrum to identify the highest peak, which provides the estimated values for heart rate and breathing rate. Fig. 2 illustrates the real-time measurement setup along with the characteristics of the radar sensor used in this study. Specifically, with a frame rate of 50 and the number of chirps set to 1, the vital signs sampling rate is 50 Hz.

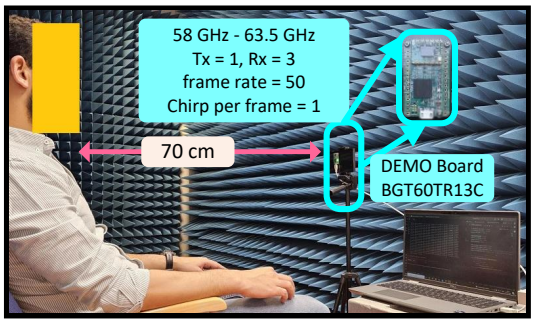

Fig. 2: Real-Time Measurement Setup for Heart and Breathing Rate Monitoring. A person sits 70 cm in front of the BGT60TR13C sensor while various phase unwrapping techniques are applied in real time. The performance of these techniques is analyzed based on the accuracy of estimated breathing and heart rates.

Mathematically, the received intermediate frequency (IF) signal in the FMCW radar, passes through the ADC, range-FFT, and range-bin selection, then it is turned into a discrete version as, $y[n] = e^{j\phi[n]}, \quad n = 1, 2, \ldots, N$, where N is the sample size in slow time. Then, the phase of the signal is estimated by $\hat{\phi}[n] = \tan^{-1}(y[n])$, where as mentioned earlier this phase is wrapped and requires to be correctly recovered. Let us define the first-order derivative of $\hat{\phi}[n]$ using the discrete difference equation, as $\delta^{(1)}[n] = \hat{\phi}[n] - \hat{\phi}[n-1]$, then, k order derivative of $\hat{\phi}[n]$ is

$$\delta^{(k)}[n] = \delta^{(k-1)}[n] - \delta^{(k-1)}[n-1],$$

with $k \in \{2, 3, \ldots, N-1\}$. In addition, $\mu_{\tilde{\delta}^{(k)}}$ is the mean of $\tilde{\delta}^{(k)}[n]$. Using these definitions, TABLE I provides a summary of the unwrapping techniques implemented for this research in a real-time application. In this table, for EATAN1 and EATAN2, "phase compensation[1]" procedure is abstracted by $\mathcal{F}(.)$. In EATAN2, r is the order of derivative calculated based on the maximum number of folds over π and $-\pi$. In addition, polynomial fitting technique is used for both EATAN1 and EATAN2 to omit the DC value of the sequence at each iteration.

III. Simulation and Measurement

Simulations and real-time measurement experiments are conducted using Python 3.12.2 and on Pycharm platform, to detect and evaluate breathing rate and heart rate simultaneously. In the simulations, vital signs are considered as sinusoidal signals [25] perturbed by RBM, which is assumed to be independent components of breathing and heart

[1]*Phase compensation in EATAN1 and EATAN2:* Let us define, $\delta^{(r-1)}[n] = \delta^{(r)}[n] - \delta^{(r)}[n-1]$ and $\bar{d}[n] = \frac{\delta^{(r-1)}[n]}{2\pi}$, Then, we set $\bar{d}[m] = \mathcal{G}^m(\bar{d}[m])$, with m as the indices where $\mathcal{I}^n_{0.5}|\mathcal{M}_1(\bar{d}[n])|$ are equal to 1. Let us define $\tilde{d}[n] = \lfloor \bar{d}[n] \rceil$, $n = 1, 2, \ldots, N$, is the rounded version of $\bar{d}[n]$ where each element turns into its nearest integer. Then, we set $\tilde{d}[\bar{m}] = 0$, here, $\bar{m}$ are the indices where $\mathcal{I}^n_{\pi}(\delta^{(r-1)}[n])$ are equal to 1. Finally, the modified unwrapped phase is defined as, $\tilde{\delta}^{(r)}[n] = \delta^{(r)}[n] - 2\pi\mathcal{S}^n_k\left(\tilde{d}[k]\right)$.

TABLE I: Summary of phase unwrapping algorithms

Method	Algorithm
PU	$\bar{\phi}[n] = \hat{\phi}[n] + \mathcal{S}^n_k\Big(\mathcal{M}_{2\pi}(\delta^{(1)}[k] + \pi) - \delta^{(1)}[k]\Big)$
MDACM [24]	$\delta^1_Q = \{Q[k] - Q[k-1]\}$ $\delta^1_I = \{I[k] - I[k-1]\}$ $\bar{\phi}[n] = \mathcal{S}^n_k\Big(I[k]\delta^1_Q - \delta^1_I Q[k]\Big)$
EATAN1 [14]	$\tilde{\delta}^{(1)}[n] = \mathcal{F}\Big(\delta^{(1)}[n]\Big)$ $\bar{\phi}[n] = \mathcal{S}^n_k\Big(\tilde{\delta}^{(1)}[n]\Big)$
EATAN2 [14]	$\tilde{\delta}^{(r)}[n] = \mathcal{F}\Big(\delta^{(r-1)}[n]\Big)$ for order $= r$ to 1 $\tilde{\delta}^{(r)}[n] = \tilde{\delta}^{(r)}[n] - \mu_{\tilde{\delta}^{(r)}}$, $\tilde{\delta}^{(r)}[n] = \mathcal{S}^n_k\Big(\tilde{\delta}^{(r)}[k]\Big)$, $\tilde{\delta}^{(r)}[n] = \tilde{\delta}^{(r)}[n] - \text{polyfit}(\tilde{\delta}^{(r)}[n])$ $\bar{\phi}[n] = \tilde{\delta}^{(r)}[n]$
UnSam [15]	Compute $\delta^{(\tilde{r})}[n]$ $\epsilon^{(0)}[n] = \mathcal{M}_\lambda(\delta^{(\tilde{r})}[n]) - \delta^{(\tilde{r})}[n]$ for $r = 0 : \tilde{r} - 2$ $\epsilon^{r+1}[n] = \mathcal{S}^n_k(\epsilon^r[n])$ $\epsilon^{r+1}[n] = 2\lambda\lceil\frac{\lfloor\epsilon^{r+1}[n]/\lambda\rceil}{2}\rceil$ $\mathcal{K}_r$ is computed based on [15]. $\epsilon^{r+1}[n] = \epsilon^{r+1}[n] + \lambda\mathcal{K}_r$ $\bar{\phi}[n] = \mathcal{S}^n_k(\epsilon^{(0)}[n]) + \bar{\phi}[n] + 2\lambda$

signals as $x[n] = x_b[n] + x_h[n] + x_r[n]$. Therein $x_b[n]$ and $x_h[n]$ are simulated as [26], $x_b[n] = \alpha_b \cos(2\pi f_b n)$, and $x_h[n] = \alpha_h \cos(2\pi f_h n)$, where α_b, f_b, α_h, and f_h, respectively, are the hypothetical amplitude and frequency of the breathing rate and heart rate signal. RBM signal is represented by $x_r[n]$ and was simulated through three different cases, including

$$x_r[n] = \begin{cases} \alpha_r \sin(2\pi f_r n_r), & \text{if sinusoidal RBM,} \\ \alpha_r n_r, & \text{if ramp RBM,} \\ \alpha_r \frac{z[n]}{||z[n]||_\infty}, & \text{if general RBM,} \end{cases}$$

where α_r, f_r and n_r are the amplitude, frequency, and duration time of RBM, consecutively. And $z[n]$ is a band-limited pseudo-noise signal at a particular frequency interval.

Simulations are conducted for vital sign signals both with and without three types of RBM. Therefore, when there are no RBM the phase is recovered using all the phase unwrapping methods mentioned in this paper; however, with the presence of RBM within some portion of the signal, which means exceeding the codomain of $[-\pi, \pi]$, methods such as UnSam and DACM can no longer properly recover the phase signal.

Fig. 3 shows the effect of RBM presence in the frequency domain, considering breathing rate and heart rate ranges of $[0.2, 0.7]$ Hz as it is depicted in yellow graphs and $[0.8, 4]$ Hz as it is shown in red graphs, respectively. Based on this figure, although all wrapping methods perform well without RBM and with ramp RBM (sub-figures (a) and (b), respectively), using EATAN1, EATAN2, and UnSam in the presence of

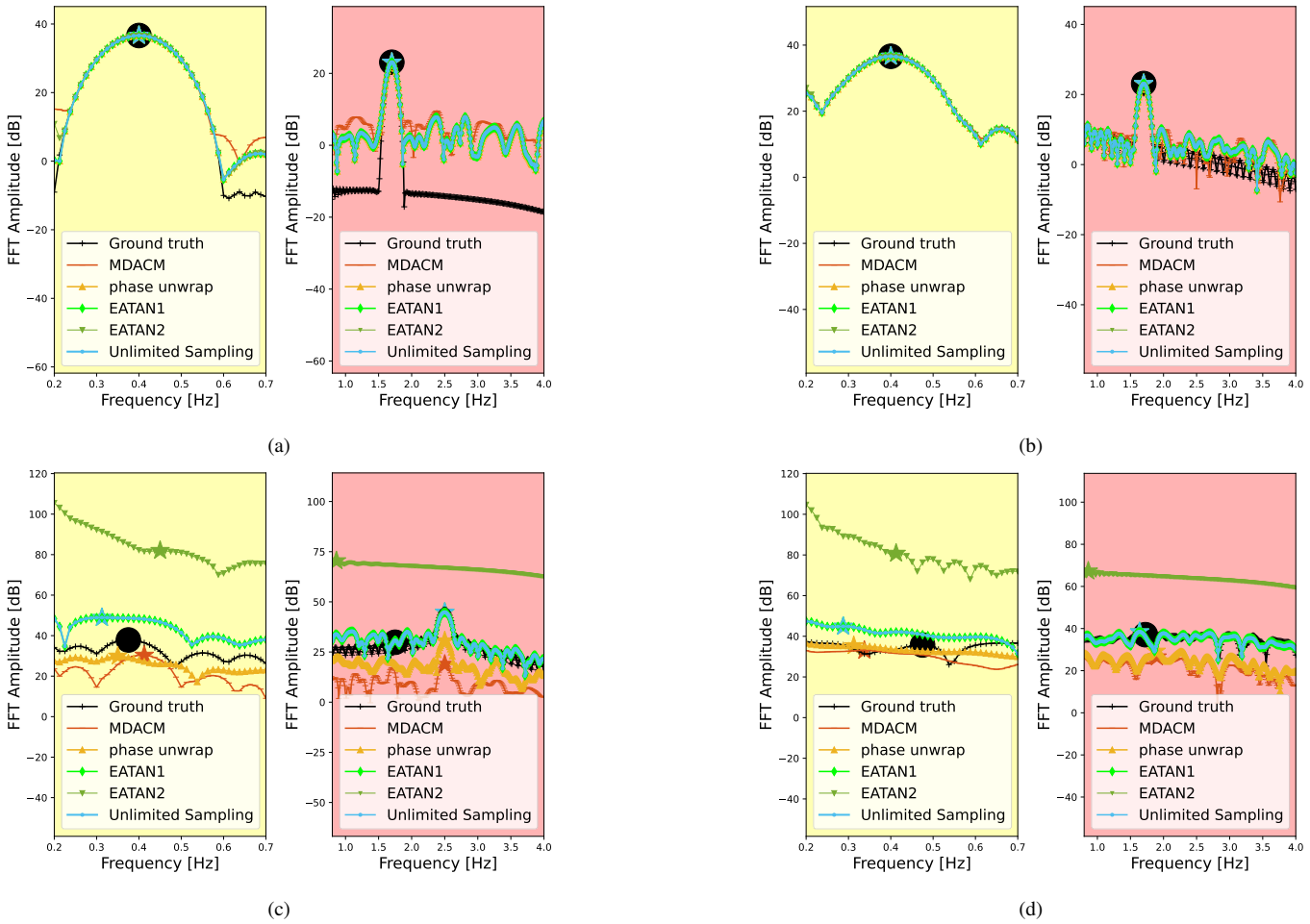

Fig. 3: (a) Vital sign signal without presence of RBM, (b) with presence of RBM ramp model, (c) sinusoidal model, and (d) general model with SNR of 20 dB in the frequency domain. Note that the yellow and pink background of the plots indicates different frequency ranges, $[0.2, 0.7]$ for breathing rate and $[0.8, 4]$ for heart rate, consecutively.

sinusoidal RBM, the estimation error increases in the breathing region (sub-figure (c)), and using EATAN2, the accuracy of the estimation of heart rate decreases. In sub-figure (d), in the general RBM condition, none of the methods can follow the ground truth peak, but in the heart interval, the recovered peak from UnSam and EATAN1 are adjacent to the ground truth peak. Fig. 4 illustrates the results of real-time measurements, with a subject positioned 70 cm in front of the radar as already depicted in Fig. 2. In this case, the accuracy of estimation for all the applied phase unwrapping techniques is almost similar when there are no RBM as indicated in sub figure (a) of Fig. 4; however, nuanced movements cause significant perturbations in all methods except MDACM and conventional PU. Consequently, no valid peak is seen in the other methods in both regions in sub-figure (b) of Fig. 4. This is due to the inherent discontinuity and noise sensitivity due to higher order differentiation in phase estimation with EATAN1, EATAN2, and UnSam, leading to ambiguity in unwrapping. The results highlight that in many practical scenarios where movement is expected, phase unwrapping methods that rely on higher-order differentiation may be vulnerable to estimation errors; thus, they are less suitable for real-world applications.

IV. Conclusion

This study evaluated the performance of various phase unwrapping methods, including PU, MDACM, EATAN1, EATAN2, and UnSam, in radar-based vital sign monitoring. Through simulations and real-time measurements, we demonstrated that PU and MDACM, which avoid the complexities associated with higher-order derivatives, exhibit superior robustness against motion artifacts induced by respiratory and cardiac movements when compared to EATAN1, EATAN2, and UnSam. Also, choosing the appropriate sampling frequency guarantees the perfect recovery in PU.

References

[1] C. Li, K.-F. Un, P.-i. Mak, Y. Chen, J.-M. Muñoz-Ferreras, Z. Yang, and R. Gómez-García, "Overview of recent development on wireless sensing circuits and systems for healthcare and biomedical applications," *IEEE Journal on Emerging and Selected Topics in Circuits and Systems*, vol. 8, no. 2, pp. 165–177, 2018.

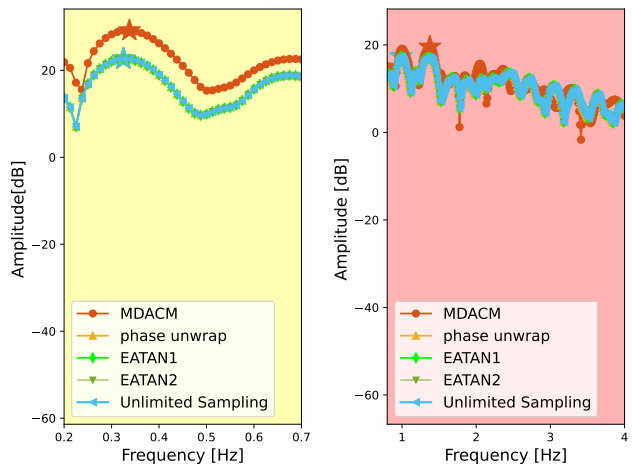

(a)

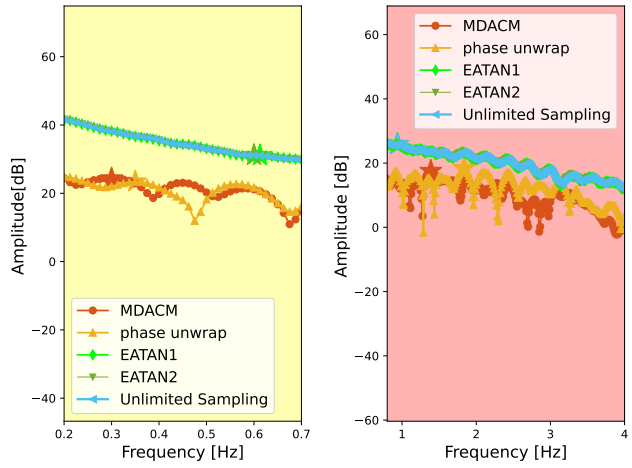

(b)

Fig. 4: (a) Vital sign signal without presence of RBM, (b) with presence of RBM in Frequency domain for real-time measurement.

[2] J. C. Lin, "Microwave sensing of physiological movement and volume change: A review," *Bioelectromagnetics*, vol. 13, no. 6, pp. 557–565, 1992.

[3] A.-J. Jang, I.-S. Lee, and J.-R. Yang, "Remote vital signal detection using ambient noise cancellation based on beam-switching doppler radar," *IEEE Transactions on Instrumentation and Measurement*, vol. 73, pp. 1–15, 2024.

[4] Y. Wang, H. Liu, W. Xiang, Y. Shui, L. Guo, M. Zhou, and Y. Pang, "A novel non-contact respiration and heartbeat detection method using frequency-modulated continuous wave radar," *IEEE Sensors Journal*, vol. 24, no. 7, pp. 10 434–10 446, 2024.

[5] Y. Eder, Z. Liu, and Y. C. Eldar, "Sparse non-contact multiple people localization and vital signs monitoring via fmcw radar," in *ICASSP 2023 - 2023 IEEE International Conference on Acoustics, Speech and Signal Processing (ICASSP)*, 2023, pp. 1–5.

[6] Z. Huo, Z. Zhang, Y. Yin, H. Chen, and Z. Shen, "Research on multitarget vital sign detection using ir-uwb radar in occlusion scenarios," *IEEE Sensors Journal*, vol. 24, no. 9, pp. 15 327–15 336, 2024.

[7] J. Möderl, E. Leitinger, F. Pernkopf, and K. Witrisal, "Variational message passing-based respiratory motion estimation and detection using radar signals," in *ICASSP 2023 - 2023 IEEE International Conference on Acoustics, Speech and Signal Processing (ICASSP)*, 2023, pp. 1–5.

[8] J. Wang, X. Wang, L. Chen, J. Huangfu, C. Li, and L. Ran, "Noncontact distance and amplitude-independent vibration measurement based on an extended dacm algorithm," *IEEE Transactions on Instrumentation and Measurement*, vol. 63, no. 1, pp. 145–153, 2014.

[9] S. Marty, A. Ronco, F. Pantanella, K. Dheman, and M. Magno, "Frequency matters: Comparative analysis of low-power fmcw radars for vital sign monitoring," *IEEE Transactions on Instrumentation and Measurement*, 2024.

[10] S. Dong, L. Wen, Y. Ye, Z. Zhang, Y. Wang, Z. Liu, Q. Cao, Y. Xu, C. Li, and C. Gu, "A review on recent advancements of biomedical radar for clinical applications," *IEEE Open Journal of Engineering in Medicine and Biology*, 2024.

[11] K. Itoh, "Analysis of the phase unwrapping problem," *Applied optics*, vol. 21, p. 2470, 07 1982.

[12] F. Schadt, F. Mohr, and M. Holzer, "Application of kalman filters as a tool for phase and frequency demodulation of IQ signals," in *2008 IEEE Region 8 International Conference on Computational Technologies in Electrical and Electronics Engineering*, 2008, pp. 421–424.

[13] L. Zhang, C.-H. Fu, Z. Zhuang, X. Yang, G. Ding, H. Hong, and X. Zhu, "Kalman filter and cross-multiply algorithm with adaptive DC offset removal," *IEEE Transactions on Instrumentation and Measurement*, vol. 71, pp. 1–10, 2022.

[14] G. Li, Y. Wang, Y. Ge, C. Guo, Q. Chen, and G. Wang, "Enhanced arctangent demodulation algorithm for periodic motion sensing with quadrature doppler radar system," *IEEE Transactions on Radar Systems*, vol. 1, pp. 230–242, 2023.

[15] A. Bhandari, F. Krahmer, and R. Raskar, "On unlimited sampling and reconstruction," *IEEE Transactions on Signal Processing*, vol. 69, pp. 3827–3839, 2021.

[16] J. Duan, J. Chen, H. Li, and Z. He, "A transformer network for phase unwrapping in fiber-optic acoustic sensors," *Journal of Lightwave Technology*, 2024.

[17] L. Kong, K. Cui, J. Shi, M. Zhu, and S. Li, "1D phase unwrapping based on the quasi-gramian matrix and deep learning for interferometric optical fiber sensing applications," *Journal of Lightwave Technology*, vol. 40, no. 1, pp. 252–261, 2022.

[18] K. Wang, L. Song, C. Wang, Z. Ren, G. Zhao, J. Dou, J. Di, G. Barbastathis, R. Zhou, J. Zhao *et al.*, "On the use of deep learning for phase recovery," *Light: Science & Applications*, vol. 13, no. 1, p. 4, 2024.

[19] M. Shin, Y. Jung, J. Kim, K. Choi, K. Lee, H. Ju, K.-I. Cho, and S. Lee, "FMCW radar-based vital signal monitoring technique using adaptive range-bin selection," in *2023 IEEE Radar Conference (RadarConf23)*, 2023, pp. 1–6.

[20] Infineon Technologies AG. (Year of access) Infineon evaluation board for bgt60tr13c. [Online]. Available: https://www.infineon.com/cms/en/product/evaluation-boards/demo-bgt60tr13c/

[21] G. Beltrão, W. A. Martins, B. Shankar M. R., M. Alaee-Kerahroodi, U. Schroeder, and D. Tatarinov, "Adaptive nonlinear least squares framework for contactless vital sign monitoring," *IEEE Transactions on Microwave Theory and Techniques*, vol. 71, no. 4, pp. 1696–1710, 2023.

[22] M. Kebe, R. Gadhafi, B. Mohammad, M. Sanduleanu, H. Saleh, and M. Al-Qutayri, "Human vital signs detection methods and potential using radars: A review," *Sensors*, vol. 20, no. 5, 2020. [Online]. Available: https://www.mdpi.com/1424-8220/20/5/1454

[23] A. De Groote, M. Wantier, G. Chéron, M. Estenne, and M. Paiva, "Chest wall motion during tidal breathing," *Journal of Applied Physiology*, vol. 83, no. 5, pp. 1531–1537, 1997.

[24] W. Xu, C. Gu, and J.-F. Mao, "Noncontact high-linear motion sensing based on a modified differentiate and cross-multiply algorithm," in *2020 IEEE/MTT-S International Microwave Symposium (IMS)*, 2020, pp. 619–622.

[25] C. Li, J. Ling, J. Li, and J. Lin, "Accurate doppler radar noncontact vital sign detection using the relax algorithm," *IEEE Transactions on Instrumentation and Measurement*, vol. 59, no. 3, pp. 687–695, 2010.

[26] D. Xu, W. Yu, Y. Wang, and M. Chen, "Vital signs detection in the presence of nonperiodic body movements," *IEEE Transactions on Instrumentation and Measurement*, vol. 73, pp. 1–16, 2024.